Universitat Politècnica de Catalunya (UPC)
Universitat Autònoma de Barcelona (UAB)
Universitat de Barcelona (UB)
Institut de Ciències Fotòniques (ICFO)

http://www.photonicsbcn.eu

Master in Photonics

MASTER THESIS WORK

QUANTUM COHERENCE AND QUANTUM CORRELATIONS

Gerard Jiménez Machado

Supervised by Prof. Dr. Juan Pérez Torres, (ICFO and UPC)

Presented on date 9th July 2017

Registered at

Escola Tècnica Superior d'Enginyeria de Telecomunicació de Barcelona

Quantum Coherence and Quantum Correlations

Gerard Jiménez Machado

ICFO, Institut de Ciències Fotòniques, Mediterranean Technology Park, 08860 Castelldefels (Barcelona), Spain

E-mail: gerard.jimenez@icfo.eu

Abstract. We demonstrate a new type of optical coherence tomography (OCT) scheme based on ideas put forward by Mandel's group in 1991 [1], curiously the same year than the first OCT scheme was demonstrated [2]. It involves the measurement of the first-order ($G^{(1)}$) correlation function between two beams that never interact with the sample under study. However, $G^{(1)}$ does depend on its reflectivity. This new scheme allows probing the sample of interest with one wavelength and measuring the coherence properties of light with another wavelength. As a result, we can gain penetration depth into the sample by using longer wavelengths, while still using the optimum wavelength for detection. We also show that $G^{(1)}$ and the degree of second-order correlation ($G^{(2)}$), between the beams that interfere and a third witness beam, are intrinsically related, showing in this way the relevant and fascinating interplay between quantum coherence and quantum correlations.

Keywords: quantum optics, optical coherence tomography, quantum coherence, quantum correlations.

1. Introduction

Coherence is one of the most fundamental aspects of electromagnetic theory, both in the classical and quantum regimes. It is a resource that can have interesting applications. In 1991, Huang et al. [2] demonstrated a new way to obtain high-resolution axial optical sectioning of a three dimensional sample. They called the new method Optical Coherence Tomography (OCT).

OCT is an interferometric technique that measures the reflectivity of each layer of the sample under study. The differentiation between light reflected from one specific layer from all other layers is done using a low-coherence source of light. This is why this method could also have been called low-coherence interferometry. Thus, the role of optical coherence in OCT is to separate one axial section (layer) of the sample from the rest, i.e., to select the measurement of reflectivity corresponding to a concrete depth inside the sample.

Here we report the experimental implementation of *a new type* of OCT, where the reflectivity of the sample is no longer directly measured. Instead it induces a change of optical coherence (first-order coherence [3]) that is indeed measured. We make

use of pairs of frequency-entangled photons generated in two separated *Spontaneous Parametric Down-Conversion* (SPDC) crystals. Coherence will be measured between signal photons ($G_{12}^{(1)}$) generated in both crystals. We will show that our scheme shows a subtle but important fundamental difference with *standard* OCT.

We will also show coincidences measurements between signal and idler photons. More specifically, we consider how second-order correlation functions ($G_{13}^{(2)}$ & $G_{23}^{(2)}$) vary as a function of the reflection coefficient of the sample that also tunes the coherence between signal photons. In other words, we want to see the interplay between quantum coherence and quantum correlations.

This thesis is organized as follows. Section 2 is dedicated to the presentation and demonstration of the new type of OCT. Firstly, we discuss the main differences between *standard* OCT and our scheme. We describe the experimental setup and show the main experimental results obtained. In Section 3 we discuss how to perform coincidence measurements in our setup, the expected results and the experimental results obtained. Finally, we summarize our conclusions.

2. Optical Coherence Tomography (OCT) with entangled photons

2.1. Our scheme vs. standard OCT

OCT is a non-invasive optical imaging technique that provides cross-sectional and axial high-resolution tomographic imaging of biological tissue [4]. Coherence plays a fundamental role in OCT, becoming a clear example where fundamental results of optical coherence theory have found an application in biomedical science. Tissues such as retina or coronary artery are the more commonly diagnosed with this technique. OCT measures the interference of light reflected back from the sample with a reference beam reflected from a mirror [2].

In standard OCT (Fig. 1), high resolution in the axial domain is achieved by making use of a Michelson interferometer (Fig. 1) and a source of light with a low coherence. The low coherence of the source is the key ingredient to obtain high-resolution in the axial direction. However, the OCT system still performs a direct measurement of the reflectivity of the sample. For each axial measurement, the two waves traversing the interferometer show coherence at the selected axial distance, with the low coherence providing the localization of the reflectivity measurement.

The inset of Fig. 1 shows a typical result of interference in an OCT scheme. As a result of interference, the output signal shows maximum and minimum of intensity as a function of the path difference between the two arms of the interferometer. If τ designates the reflectivity of a particular layer of the sample, the visibility of the interference pattern is

$$V = \frac{\mathrm{I_{max}} - \mathrm{I_{min}}}{\mathrm{I_{max}} + \mathrm{I_{min}}} = \frac{2|\tau|}{1 + |\tau|^2}, \tag{1}$$

where $\mathrm{I_{max}}$ and $\mathrm{I_{min}}$ are the maximum and minimum intensities detected after the BS. The bandwidth of the source, and thus its coherence length, determines the axial

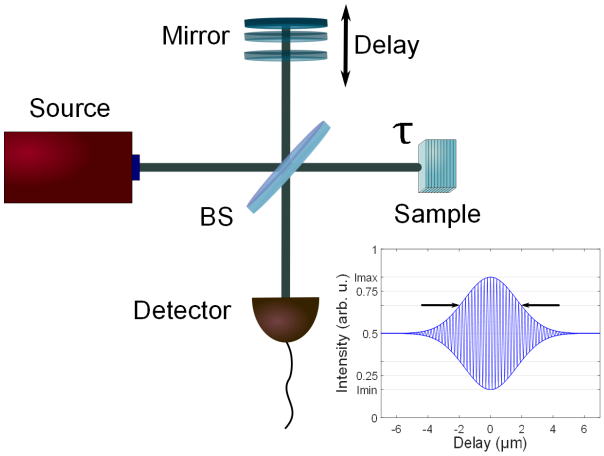

Figure 1: Standard OCT scheme and typical interferogram that is the result of a measurement. In this particular case, we have chosen a visibility of V=60% and an axial resolution of approximately 3.5 μm.

resolution of the measurement.

Our OCT system, that we demonstrate experimentally, is based on the concept of induced coherence, an idea put forward in 1991 by Zou et al. [1]. In their experiments, a pump beam is divided to pump two spontaneous parametric down-conversion (SPDC) sources, where one pair of signal/idler photons can be generated. The interference pattern appears when the two signal photon arms are recombined, only if the idler photons become indistinguishable. The degree of distinguishability of the idler photons generated in each nonlinear crystal, and its effect on the nature of the interference pattern of signal photons, is commonly called *which-way* information. So, if we cannot differentiate the two idlers, there is no way to know in which of the two arms we have generated the signal photons unless the reflectivity of the sample introduces such distinguishability.

The reflectivity of the sample translates into a loss of coherence between the lights beams traveling the two arms of the interferometer. This loss of coherence is the quantity that is measured. Therefore in our system we measure coherence instead of reflectivity, even though this loss of coherence can be related linearly to the reflectivity of the sample.

Fig. 2 summarizes schematically the main differences between *standard* OCT, an imaging system that measures reflectivity, and our tomography scheme, a system that measures the loss of coherence induced by the presence of a reflectivity different from 1.

Our technique does not require the laser or the detector to work at the same wavelength as that of the light interacting with the object. Then, information of the object is obtained without detecting the photons that interacted with it.

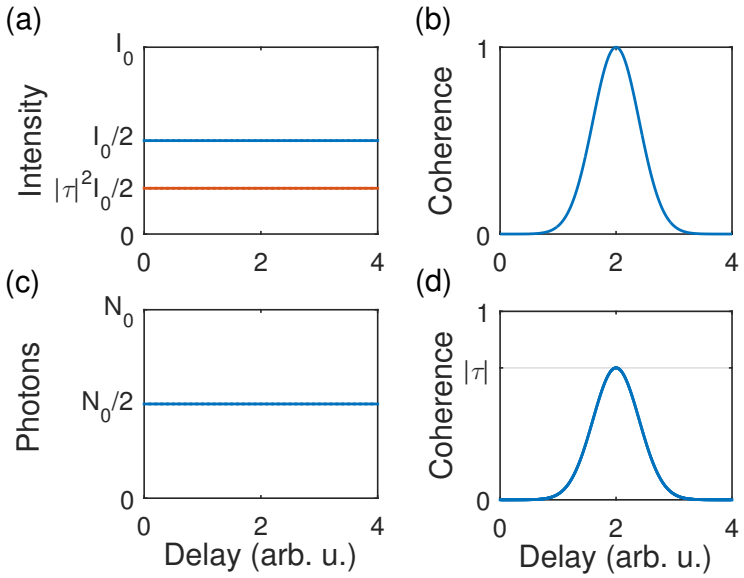

Figure 2: Subtle difference between the way *standard* OCT works [see (a) and (b)], and how it works our OCT scheme [see (c) and (d)]. (a) & (c): Plot of the intensity (or photon flux) traversing the two arms of the interferometer. (b) & (d) Degree of coherence between the light beams propagating in the two arms of the interferometer.

2.2. Experimental setup

Our setup can be understood as a nonlinear interferometer composed of two identical nonlinear crystals located in the two arms of the interferometer. A high-power continuous-wave laser beam (pump) Verdi V10 interacts with two nonlinear crystals, leading to the probabilistic formation of frequency-entangled photon pairs through the process of SPDC. Only signal photons traverse the interferometer and only idler photons interact with the sample.

The pump beam is split with a 50:50 beam splitter (BSp). Two Type-0 periodically-polled lithium niobate (PPLN) nonlinear crystals are located in each arm of the interferometer and mounted on top of ovens. They absorb with very low probability a 532 nm pump photon and re-emit two lower-frequency photons, signal (810 nm) and idler (1550 nm). The signal and idler photons are separated by two dichroic mirrors ($DM_{1,2}$), where the 810 nm signal photons are transmitted, forming the two arms of the Mach-Zehnder interferometer. Both are recombined in the polarization beam splitter (PBS_2).

The 1550 nm idler photon coming from $PPLN_1$ is reflected in the dichroic mirror DM_1. It is reflected again in the polarization beam splitter (PBS_1). Then interacts with the sample, formed by a variable neutral density filter (NDF) and a mirror. This photon, now carrying the information of the sample (reflectivity τ), is transmitted through the PBS_1 this time. With another dichroic mirror DM_1, this idler photon has to be spatially overlapped with the pump beam that impinges on the second nonlinear crystal, and consequently also with the second 1550 nm idler photon.

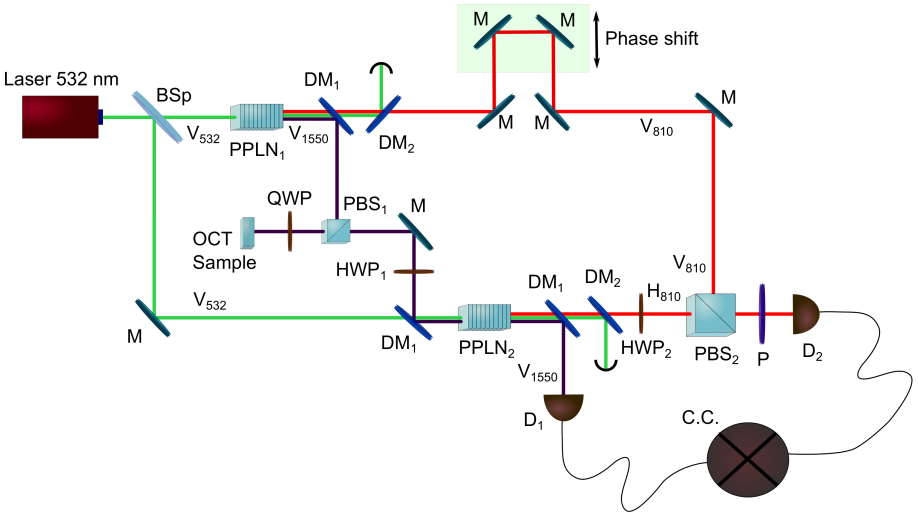

Figure 3: Experimental setup aimed at observing optical coherence and quantum correlations. In order to measure the first-order coherence function, we only use one the single-photon detector D_2. For measuring second-order correlation functions, we use detectors D_1 and D_2.

The second 810 nm signal photon traverses the lower interferometer arm until it reaches PBS_2. A delay is introduced in one of the two arms, formed by two mirrors implemented on top of a platform able to perform steps of 30 nm thanks to a 6-mm stepper motor (Thorlabs Z806) attached to it. Finally, the beam resulting from the combination of the two signal photons is coupled into a single mode fibre and measured with a silicon based single photon detectors (Perkin-Elmer SPCM-AQR Single Photon Counting Module).

2.3. Experimental results

The results obtained with our experimental setup constitute a *proof-of-concept* of the idea of *optical coherence tomography with entangled photons*. Figure 4(a) shows the measurement of the degree of first-order coherence between signal photons, when the idler photon generated in the first nonlinear crystal is reflected from a mirror ($|\tau| = 1$) that can be moved between two positions. The resulting measurement curve shows clearly the corresponding coherence function shapes simulating a two-layer system where the layers are separated 1 mm apart.

The coherence length and shape of the coherence functions are directly related with the shape and bandwidth of the emitting source, shown in Fig. 4(b). In our case, the 20-mm-long PPLN type-0 crystal generates a SPDC idler spectral emission bandwidth of about 1.6 nm at FWHM, measured with an optical spectrum analyser (OSA), corresponding to approximately 0.5-mm axial resolution in the interferometric measurements.

In Fig. 5(a) we show the number of signal photons detected at the output of PBS_2

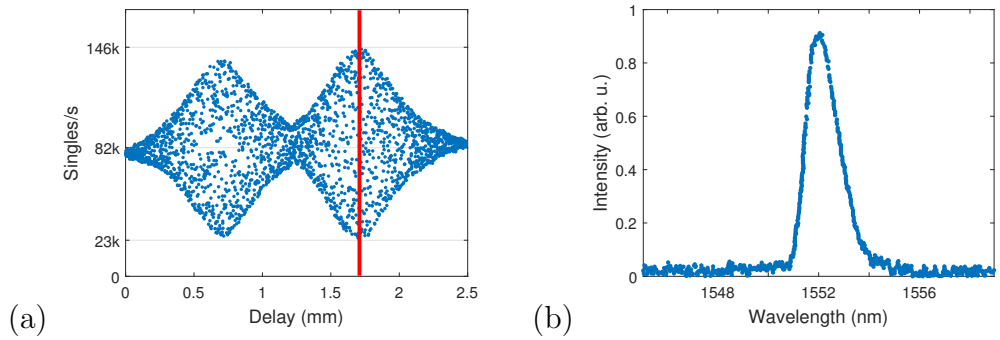

Figure 4: Experimental *optical coherence tomography* results. (a) Degree of coherence measured for an object that consist of two layers separated 1 mm apart. We detect the signal photons at the output of BSs. We change the path difference by micrometric steps of $1\,\mu$m, obtaining a maximum visibility of $V = 71.2\%$ (in red). (b) Frequency spectrum of the SPDC idler photon.

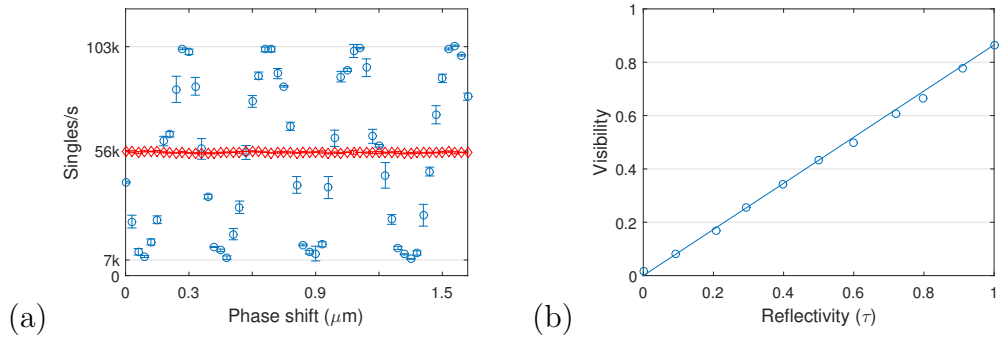

Figure 5: (a) Interference fringes for two different values of the reflection coefficient. Circles: $|\tau| = 1$; Diamonds: $|\tau| = 0$. The maximum visibility measured is $V = 86.5\%$. The error bars designate the standard deviation of the experimental measures. (b) Experimental and theoretical relationship between the interference pattern visibility and the reflectivity (τ). Circles: experimental data; Solid curve: theoretical prediction.

changing the length of one arm with respect to the other by 30 nanometer steps. In red (diamonds) we show the effect of blocking the first 1550 nm idler photon arm, that corresponds to a sample with zero reflectivity, $|\tau| = 0$. Finally, Fig.5(b) depicts the experimental relationship between the visibility of the interference pattern and the reflectivity. The value of τ is introduced by a variable neutral density filter (NDF) in the path of the first 1550 nm idler photon.

3. Coherence and correlations

We measure now correlations between the signal photons and the idler generated in the two SPDC sources. That is, we perform coincidence measurements between photons signal and idler as it is shown in Fig. 3. More specifically, we want to measure the

second-order correlation function of the signal photon generated in the first nonlinear crystal with the idler ($g_{13}^{(2)}$) and the same for the signal photon emitted from the second one with the idler ($g_{23}^{(2)}$). And we want to do it as a function of the reflectivity of the lossy system.

The theoretical expressions of the normalized second-order correlation functions are

$$g_{13}^{(2)} = 1 + \frac{|\tau|^2}{1+|\tau|^2}\frac{B}{R}, \tag{2}$$

and

$$g_{23}^{(2)} = 1 + \frac{1}{1+|\tau|^2}\frac{B}{R}, \tag{3}$$

for a temporal delay between signal and idler photons smaller than $1/B$, $g_{13}^{(2)} = g_{23}^{(2)} = 1$ otherwise. Here τ is the reflection coefficient, B is the bandwidth of SPDC and R is the flux rate of down-converted photons [5, 6].

In an experimental set-up, the rate of coincidence counts R_{12} in a detection time T_R is [7]

$$R_{12} = \eta_{12}\int d\tau < a_s^\dagger(t)a_i^\dagger(t+\tau)a_i(t+\tau)a_s(t) >= \frac{\eta_{12}}{\eta_1\eta_2}R_1R_2T_R[1+\frac{T_c}{T_R}\frac{B}{R}], \tag{4}$$

where η_{12} is the efficiency of coincidence detection, $R_{1,2} = \eta_{1,2}S_{1,2}$ is the measured singles flux-rate, $\eta_{1,2}$ are singles efficiencies and we write $g^{(2)}(\tau) = 1+\gamma(\tau)$. Therefore:

$$\gamma(0) = \frac{R_{12} - \eta R_1R_2T_R}{\eta R_1R_2T_c}, \tag{5}$$

where $\eta = \eta_{12}/(\eta_1\eta_2)$.

3.1. Experimental setup

A photon coincidence measurement is understood as a simultaneous detection in two (or more) different photodetectors. Thus it is really important to control the path lengths (i.e. temporal delay) between them. For this, we have to take into account every stage that the photons follow and to calculate the time that they take in each of them. Essentially, in our case, the temporal delays to take into account are due to: the optical path, optical fibers, the coaxial cable and the temporal response of the photodetectors.

We use two different photodetectors: Perkin-Elmer SPCM-AQR Single Photon Counting Module (for the signal photons at 810 nm) and idQuantique id201 Single Photon Detection Module (for the idler photons at 1550 nm). The coincidence measurements are performed in the following way: the output detection of the Perkin-Elmer triggers the detection in the idQuantique photodetector, measuring directly the coincidences (Fig. 6). Thus the following condition must be fulfilled:

$$t_{idler} \geq t_{signal} + 8ns \tag{6}$$

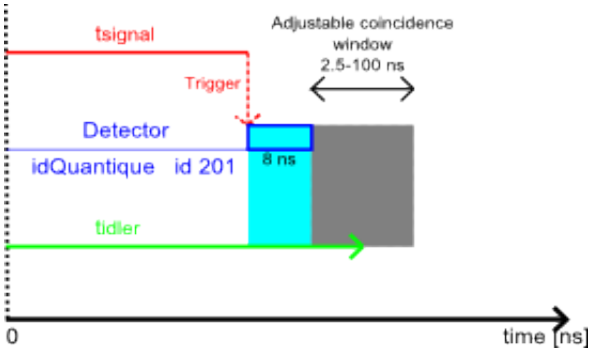

Figure 6: Temporal lines for both photons and the idQuantique id201 detector.

We have to adjust the idler photon time in order to make it *fall* inside the so called coincidence window. For this, we use the appropriate combination of optical fibre and BNC cable just to avoid changes in the optical path. Furthermore, from Eq. (4, 5) [8] we derive that for a fixed temporal detection window T_R, we need to use flux rates as small as possible ($RT_R << 1$) and total detection windows (T_0) as long as possible ($T_0 >> T_R$).

3.2. Experimental results

We have performed coincidences measurements following the scheme and constraints explained in the previous subsection. Concretely, the experimental settings that we used are summarized in the following list:

- Single mode fibers lengths: $l_{idler} = 12m$ and $l_{signal} = 2m$
- BNC cable length: $l_{BNC} = 0.40m$
- Temporal detection (coincidence) window: $T_R = 2.5ns$
- Total detection window: $T_0 = 30s$
- Trigger (signal) rate: $R_1 = 2000Hz$
- Idler rate: $R_2 = 2000Hz$

Fig. 7 shows the coincidences counts (R_{12}) measured as a function of the delay between the signal photons and the idler one, for different values of the reflection coefficient (τ). We can see that the coincidence counts between photon generated in the second crystal do not depend on the reflection coefficient. This is completely different for the signal photon generated in the first crystal and the idler, since we are affecting directly the signal-idler correlation by changing the reflectivity.

From measurements of R_{12}, R_1, R_2 and R_3 we can calculate $\gamma(0)$ for each reflection coefficient. Finally, we plot the normalized second-order correlation functions $g_{13}^{(2)}$ and $g_{23}^{(2)}$ as a function of the reflection coefficient (Fig. 8).

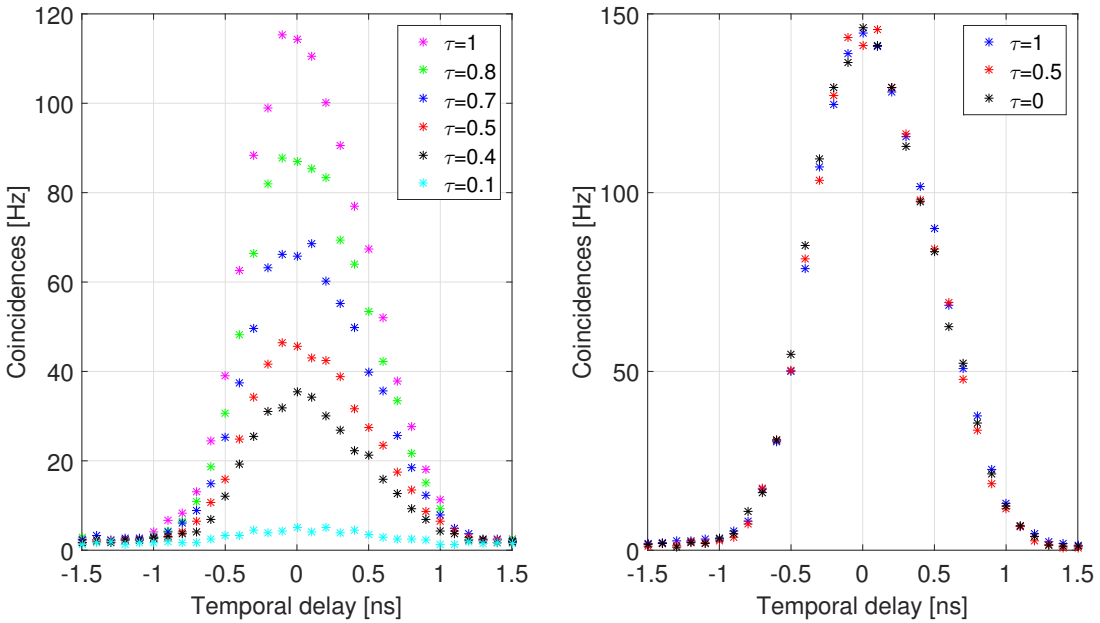

Figure 7: Measured coincidences counts (R_{12}) for different values of the reflection coefficient (τ) as a function of the temporal delay. LEFT: Coincidences counts between signal photons traversing the upper arm of the interferometer and idler photons. RIGHT: Coincidences counts rate between signal photons traversing the lower arm of the interferometer and idler photons.

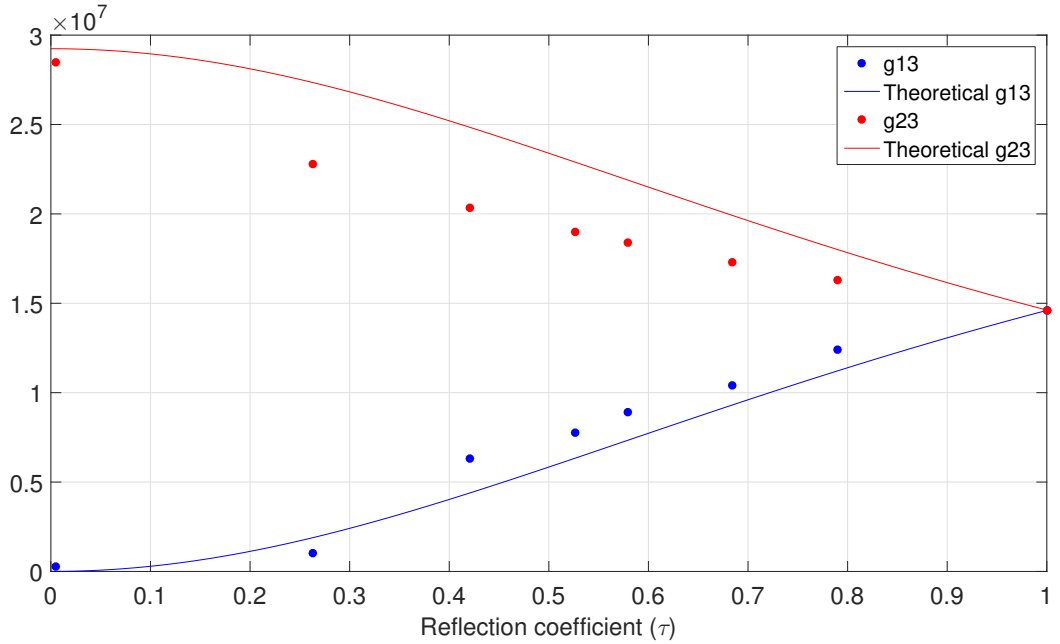

Figure 8: Normalized second-order correlation functions ($g^{(2)}_{13}$ and $g^{(2)}_{23}$) dependence on the reflection coefficient (τ). The blue dots correspond to calculated values from experimental data of $g^{(2)}_{13}$ and the red ones for $g^{(2)}_{23}$. The theoretical curve [Eqs. (2) and (3)] make use of the measured values $R = 2000Hz$ and $B = 1/580$ fs.

4. Conclusions

In this work, we report a new type of optical coherence tomography (OCT) scheme. In our approach we measure coherence, whose value depends on the reflectivity of the sample, i.e., the change of reflectivity induces a direct change of the coherence of two streams of photons that are made to interfere. One remarkable advantage of our scheme is that it allows to detect photons at wavelengths that show maximum efficiency of silicon detectors, while the sample is being probed with photons in the telecom band, that can penetrate deeper into biological tissue.

Moreover, we have demonstrated a profound link between coherence (first-order correlation function) and correlations (second-order correlation function). We have measured the dependence of the normalized second-order correlation functions ($g_{13}^{(2)}$ & $g_{23}^{(2)}$) with the reflection coefficient of a lossy system, that also tunes the degree of coherence between signal photons. Which-path information can be quantified by how much difference there is between $g_{13}^{(2)}$ and $g_{23}^{(2)}$, that also determines the amount of coherence present between signal photons. This constitute a beautiful bridge between two fundamental theoretical aspects on quantum optics: coherence and correlations.

Acknowledgments

First of all, my great appreciation goes to my supervisor, Professor Dr. Juan Pérez Torres, for giving me the opportunity to study in his quantum optics group at ICFO during the last year. I would also like to specially acknowledge Adam Vallés for instructing me all his limitless laboratory knowledge and for his crucial contribution in the building of the setup and measuring the results. I also want to thank to my group mates Luís José Salazar, Lluc Sendra and Job Mendoza for making ICFO a nice and pleasant place.

Bibliography

[1] X. Y. Zou, L. Wang, and L. Mandel, "Induced coherence and indistinguishability in optical interference," *Phys. Rev. Lett.*, vol. 67, p. 318, 1991.

[2] D. Huang, E. Swanson, C. Lin, J. Schuman, W. Stinsona, W. Chang, M. Hee, T. Flotte, K. Gregory, C. Puliafito, and et. al., "Optical coherence tomography," *Science*, vol. 254, p. 1178, 1991.

[3] R. J. Glauber, "The Quantum Theory of Optical Coherence," *Phys. Rev.*, vol. 130, p. 2529, 1963.

[4] A. Fercher, W. Drexler, C. Hitzenberger, and T. Lasser, "Optical coherence tomography principles and applications," *Rep. Prog. Phys.*, vol. 66, pp. 239–303, 2003.

[5] J. P. Torres, K. Banaszek, and I. A. Walmsley, "Engineering nonlinear optics sources of photonic entanglement," *Prog. Optics 56*, p. 227, 2011.

[6] V. Balic, D. Brage, P. Kolchin, G. Y. Yin, and S. E. Harris, "Generation of paired photons with controllable waveforms," *Phys. Rev. Lett. 94*, vol. 183601, 2005.

[7] E. Wolf and L. Mandel, "Coherence and quantum optics," vol. Section 14.7.2, Eq. 14.7-3.

[8] X. Y. Ou, L. J. Wang, and L. Mandel, "Violation of classical probability parametric down-conversion," *Opt. Comm. 84*, p. 351, 1991.